

Phase-Stable Self-Modulation of an Electron Beam in a Magnetic Wiggler

James P. MacArthur,^{1,2,*} Joseph Duris,¹ Zhen Zhang,¹ Alberto Lutman,¹ Alexander Zholents,³ Xinlu Xu,¹ Zhirong Huang,^{1,2} and Agostino Marinelli^{1,2,†}

¹SLAC National Accelerator Laboratory, Menlo Park, California 94025, USA

²Stanford University, Stanford, California 94305, USA

³Argonne National Laboratory, Lemont, Illinois 60439, USA

 (Received 17 May 2019; revised manuscript received 26 September 2019; published 20 November 2019)

Electron beams with a sinusoidal energy modulation have the potential to emit subfemtosecond x-ray pulses in a free-electron laser. An energy modulation can be generated by overlapping a powerful infrared laser with an electron beam in a magnetic wiggler. We report on a new infrared source for this modulation, coherent radiation from the electron beam itself. In this self-modulation process, the current spike on the tail of the electron beam radiates coherently at the resonant wavelength of the wiggler, producing a six-period carrier-envelope-phase (CEP)-stable infrared field with gigawatt power. This field creates a few MeV, phase-stable modulation in the electron-beam core. The modulated electron beam is immediately useful for generating subfemtosecond x-ray pulses at any machine repetition rate, and the CEP-stable infrared field may find application as an experimental pump or timing diagnostic.

The first generation of x-ray free-electron lasers has now operated for a decade [1–5], supplying gigawatt x-ray beams to a variety of users [6]. These facilities typically generate self-amplified spontaneous emission (SASE), a lasing process which produces longitudinally incoherent beams whose spectral widths lie in the range of $\Delta\omega/\omega \approx 10^{-3}$ – 10^{-4} [7,8] and whose longitudinal signatures match that of the electron-beam current at a few to hundreds of femtoseconds in duration. There is interest from the community of x-ray laser users in pulses capable of probing phenomena with subfemtosecond resolution [9,10]. Successful experimental efforts [11–17] toward this goal have yet to break the subfemtosecond barrier at soft x-ray energies.

Single-spike, subfemtosecond x-ray beams may be produced by electron beams with a nearly single-cycle energy modulation [18–21]. These beams could be generated by overlapping a single-cycle carrier-envelope-phase (CEP) stable laser with an electron beam in a wiggler [22]. Suitable infrared lasers exist [23], but challenges in optical transport and laser-electron synchronization hinder progress.

In this Letter, we demonstrate that an electron beam may be modulated in a six-period wiggler with no external laser present at the Linac Coherent Light Source (LCLS). Instead, coherent radiation from a current spike on the electron-beam tail creates a quasi-single-cycle energy modulation in the beam core. The modulation exhibits subfemtosecond stability and is a few MeV in amplitude, in agreement with a line-charge model [24–26], a paraxial model developed in the Supplemental Material [27], and the 3D code OSIRIS [32]. These beam characteristics are

sufficient for enhanced-SASE operation at any repetition rate. A six-cycle, CEP-stable, gigawatt infrared pulse is a byproduct of this process. The pulse is timed with subfemtosecond precision relative to the electron beam, and it could therefore be used as timing fiducial or in pump-probe experiments.

A schematic of our experiment is shown in Fig. 1. A beam of electrons with relativistic factor γ travels left to

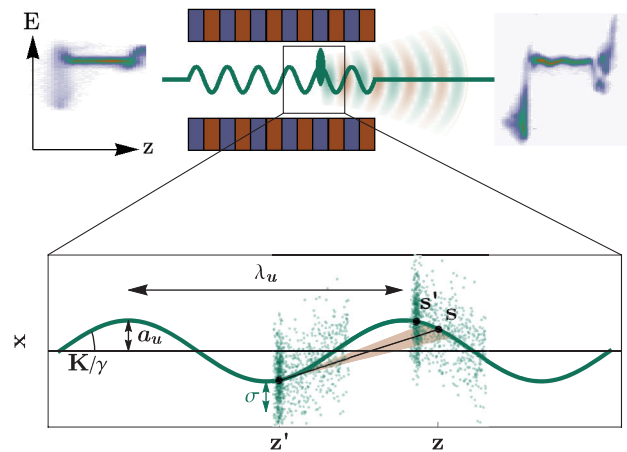


FIG. 1. (Top panel) An electron beam enters a six-period wiggler. Radiation generated in the wiggler interacts with the beam, producing a sinusoidally modulated phase space. (Bottom panel) Inside the wiggler, a single electron beam (green dots) of rms width σ traverses a sinusoidal path of amplitude a_u from left to right. The high current tail slice of the beam, s' , emits radiation at the longitudinal position z' that reaches a core slice s at the longitudinal position z .

right along a sinusoidal path (green) of wavelength $\lambda_u = 2\pi/k_u$ within a six-period planar wiggler. The resonant wavelength in the wiggler is

$$\lambda_1 = \frac{\lambda_u}{2\gamma^2} \left(1 + \frac{K^2}{2}\right) \approx \frac{\lambda_u K^2}{4\gamma^2}, \quad (1)$$

where the planar wiggler deflection parameter, K , satisfies $1 \ll K \ll \gamma$. The tail of the electron bunch, a current spike shorter than the resonant wavelength in the wiggler, emits coherently at the wavelength $\lambda_1 = 2\pi/k_1$. This radiation resonantly modulates the beam core as it slips ahead of the electrons.

When the oscillation amplitude, $a_u = K/\gamma k_u \approx \sqrt{\lambda_u \lambda_1}/\pi$, is much larger than the transverse beam-width, 2σ ,

$$\hat{\sigma} = 2\sigma/a_u = \sigma\sqrt{k_1 k_u} \ll 1, \quad (2)$$

a line-charge model developed from the Liénard-Wiechert fields [24–26] adequately describes the self-modulation process. This model includes short-range space-charge-like effects and long-range radiative effects [33]. The line-charge limit is relevant to our experiment, wherein $\hat{\sigma} \sim 0.4$.

In reference to Fig. 1, we are interested in calculating the energy modulation at the longitudinal beam coordinate s in response to N_e electrons concentrated on the beam tail at $s = 0$. In an infinite planar wiggler with $K \gg 1$, the wiggler-period-averaged relative energy change grows in proportion to the propagation distance z along the wiggler [26],

$$\Delta\gamma(z, s) = -r_e N_e z w(s), \quad (3)$$

where r_e is the classical electron radius, and $w(s)$ is the point-charge longitudinal wake function derived elsewhere [26] and reproduced in the Supplemental Material [27].

The universal planar wiggler wake function, $-4w(k_1 s)/(k_1 k_u)$, is reproduced from Ref. [26] in Fig. 2. In writing Eq. (3), we have assumed an electron line density of $\lambda(s) = N_e \delta(s)$. This impulse response may be convolved

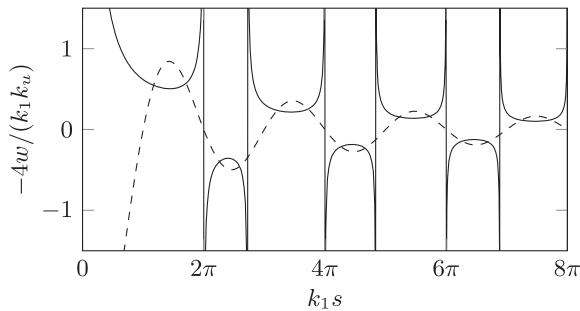


FIG. 2. The planar wiggler wake function (solid) and the first-harmonic contribution to the wake function (dashed). This is the wake of a point source at $s = 0$, and it is nonzero for test charges ahead of the source, $s > 0$.

with a measured electron probability density to predict the modulation along a realistic beam profile. In our experiment, modulation at the first harmonic is dominant in the beam core since the current spike on the tail is larger than $\lambda_1/3$ in extent. The long-range first-harmonic contribution to the energy modulation is

$$\Delta\gamma_1(z, s) = -2r_e N_e z [JJ]^2 k_1 k_u \text{sinc}(k_1 s), \quad (4)$$

where $[JJ] = J_0[1/(2+4/K^2)] - J_1[1/(2+4/K^2)] \approx 0.696$. This expression is derived in the Supplemental Material [27]. The first-harmonic contribution to the universal wiggler wake function is also shown in Fig. 2.

The quasi-single-cycle nature of the energy modulation in the beam core is a result of the denominator in $\text{sinc}(k_1 s) = \sin(k_1 s)/(k_1 s)$. The physical source of this term is the strong diffraction of radiation produced by the beam tail. The modulation may easily exceed a few MeV near $s = 0$ if enough charge is concentrated in the electron-beam tail. For example, an electron-beam tail containing $N_e = 50$ pC/e electrons traveling through a wiggler configured as in Table I will generate a modulation of amplitude $2r_e N_e z [JJ]^2 k_1 k_u / (2\pi) \approx 9$, or 4.5 MeV, at $k_1 s = 2\pi$.

We want to emphasize the importance of a small scaled beam size, $\hat{\sigma}$, in preserving this large modulation amplitude. In the Supplemental Material [27], we solve for the energy modulation in a finite wiggler under the paraxial approximation with a nonzero $\hat{\sigma}$. We show that the modulation amplitude scales as $1/\hat{\sigma}^2$ for large $\hat{\sigma}$. We also demonstrate that the modulation amplitude in a noninfinite wiggler is slightly reduced from the infinite wiggler modulation amplitude. This reduction is a result of the shortened interaction length for slices of the bunch far from the tail.

Self-modulation was observed experimentally using an X-band transverse deflecting cavity (XTCAV) [34] at the LCLS. The LCLS current profile has spikes at the head and tail of the bunch that are typically suppressed with two collimators in a dispersive section [35]. In this experiment, we remove one collimator to maximize the peak current in the tail. In Fig. 3, the electron-beam phase space from an XTCAV measurement is projected onto the longitudinal

TABLE I. Wiggler and electron-beam parameters.

Parameter	Figures 3 and 4	Figure 5	Figure 6
Wiggler gap (mm)	8.2	8.2	11.5
Wiggler K value ^a	51.5	51.5	43.3
Wiggler period (cm)	35	35	35
Wiggler length ^b (cm)	230	230	230
Beam energy ^c (MeV)	3953	3782	3420
Beam charge ^c (pC)	200	180	140

^aCalculated from Hall-probe field maps.

^bIncludes fringe fields; effective magnetic length is six periods.

^cReported values are set points; actual values vary shot to shot.

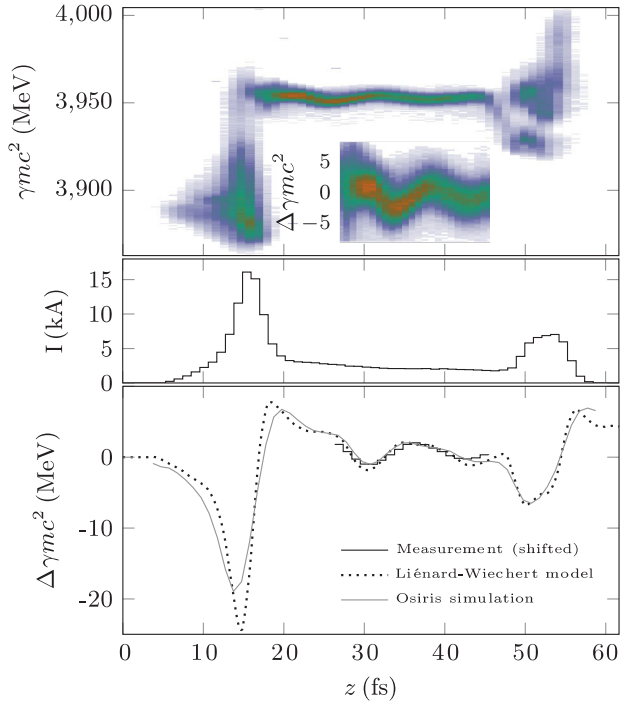


FIG. 3. (Top panel) The measured transverse phase space of a modulated electron beam with the tail to the left. (Inset) The beam core. (Middle panel) A projection onto the time axis yields the current profile. (Bottom panel) The energy modulation predicted from the Liénard-Wiechert line-charge model (dotted) and the OSIRIS simulation (gray) match the shifted measurement data (black).

axis to reveal a high current spike on the electron-beam tail. Wiggler and beam parameters are given in Table I. This current profile is convolved with the line-charge model, Eq. (3), to generate the predicted modulation profile. We note that the compression factor, $R_{56} = \gamma \Delta s / \Delta \gamma$, of the wiggler perturbs the current profile over six periods, a phenomenon not accounted for in this model. This effect is important for longer wigglers [36].

We also performed a simulation of the self-modulation process in the average beam rest frame using the 3D particle-in-cell code OSIRIS [32]. In this boosted frame, the wiggler period and resonant wavelength are equal, a convenience that allows all relevant quantities to be resolved on the same simulation grid [37–39]. Our simulation inputs were the current distribution in Fig. 3, a 2 MeV rms slice energy spread, a beam size of $\hat{\sigma} = 0.4$, a normalized emittance of $0.4 \mu\text{m}$, and the wiggler parameters given in Table I. The simulation time step and grid size were set to resolve short-range effects, $dx = dy = dz = 2c dt = 1/(16k'_1)$, with k'_1 representing the resonant wave number in the average rest frame. The average rest frame is boosted along the z axis by a Lorentz factor of $\gamma_z = \gamma/\sqrt{1 + K^2/2} = 212.3$ relative to the lab frame. The output energy modulation is in close agreement with the line-charge model.

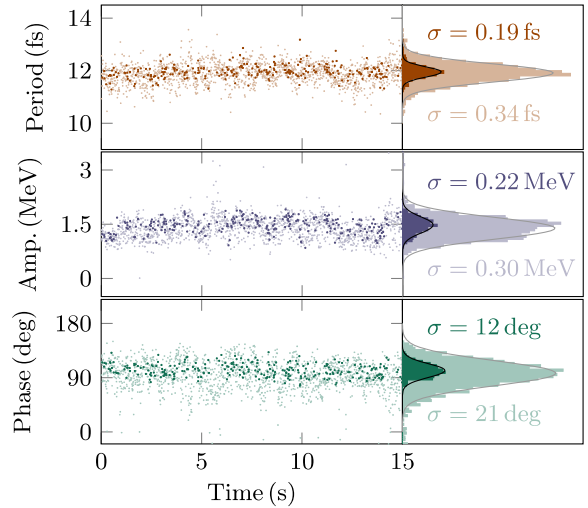


FIG. 4. The best fit modulation period (top panels), amplitude (middle panels), and phase (bottom panels) for consecutive pulses in a 15 s time frame. The rms width of a Gaussian fit to the binned data is also reported (right panels), for both the entire dataset (light), and a dataset where the peak current in the second bunch compressor is restricted (dark).

The measured energy modulation from XTCAV is shown in Fig. 3 for comparison with the simulation and the line-charge model. Owing to challenges in reconstructing the exact phase space before the wiggler, the data were shifted vertically and horizontally for comparison purposes. Only the modulation amplitude and wavelength should be inferred from these data.

To demonstrate the stability of self-modulation, we measure the variation in the modulation period, amplitude, and phase relative to the current spike for a series of 1800 consecutive shots in Fig. 4. The raw rms modulation period variation is 340 as. Much of this variability is due to the 1.06 fs temporal resolution of the TCAV and linear particle accelerator (linac) jitter that modifies the peak current on a shot-by-shot basis. After filtering by the peak current as measured in the second bunch compressor, the rms period variability drops to 190 as. Similar improvements are seen in the modulation amplitude and phase. The intrinsic stability of the self-modulation process makes it a reliable replacement for modulation from an external laser.

As demonstrated in Fig. 3, the beam tail has a large energy spread [35]. This means that the peak current in the tail may be controlled with R_{56} adjustments between the linac and wiggler in a dispersive section called dog-leg 2 [40]. In Fig. 5, we provide an example of wagging the beam tail in dog-leg 2. With the near-optimal R_{56} of -0.15 mm in Fig. 5(b), the modulation amplitude in the beam core is largest. The overcompressed beam tail of Fig. 5(a) and the undercompressed tail of Fig. 5(c) yield a smaller modulation amplitude in the beam core.

A by-product of the self-modulation process is a six-period, CEP-stable infrared light pulse at the resonant

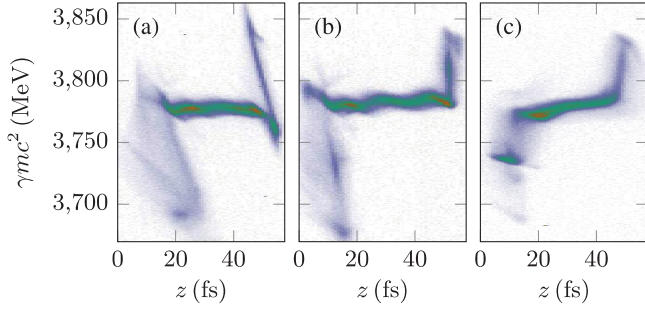


FIG. 5. The electron-beam phase space as measured in the dump when the dog-leg 2 (a) $R_{56} = -0.25$ mm, (b) $R_{56} = -0.215$ mm, and (c) $R_{56} = 0.2$ mm. Tail is to the left.

wavelength of the wiggler. The radiated pulse energy can be estimated by measuring the average energy loss of the electron beam as it travels through the wiggler. Figure 6 shows the average bunch energy measured in the dump for 4000 consecutive shots with the wiggler set to $K = 43.3$ (red) and $K = 0$ (blue). The data are distributed along the horizontal axis according to the beam position in a dispersive portion of the linac upstream from the wiggler. This helps distinguish between energy lost in the wiggler and shot-to-shot energy fluctuations that produce energy-correlated orbits. With the wiggler out, the average beam energy is larger by 2 MeV per electron, in rough agreement with the 4.3 MeV energy loss from the idealized OSIRIS simulation. We note that our set point optimized the stability of the beam-core energy modulation, but not the energy loss. We operate close to, but not at, full compression of the beam tail in the wiggler. This produces more energy loss at nonzero dispersive positions in Fig. 6, where additional R_{56} changes the current profile.

The 2 MeV energy loss and a charge of 140 pC imply an infrared pulse with 280 μJ , or roughly 4 GW over six

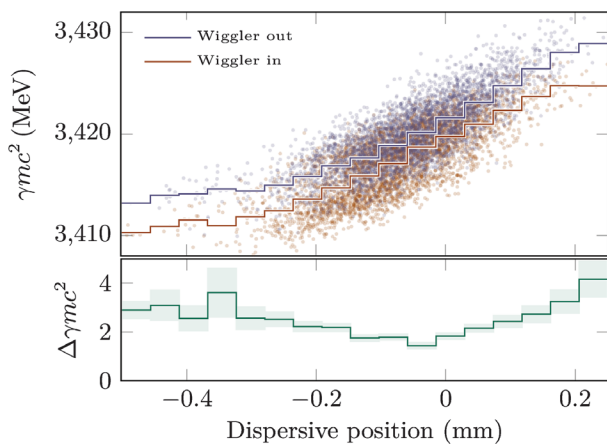


FIG. 6. (Top panel) The average beam energy is plotted as a function of position in a dispersive region of the linac to undulator transport line when the wiggler is out (blue) and in (red). (Bottom panel) The few MeV difference between the binned distributions is shown with $1 - \sigma$ error bars.

periods, is produced every shot. Note that, while the beam modulation exhibits a quasi-single-cycle temporal structure, the paraxial model introduced in the Supplemental Material [27] predicts that the IR pulse is composed of 6 cycles with a uniform power profile in time. The pulse bandwidth is therefore $\Delta\lambda/\lambda \sim 1/6$.

A pulse energy of 280 μJ is comparable to dedicated infrared sources available to LCLS users [41]. This pulse comes with subfemtosecond timing precision relative to the electron beam at any linac repetition rate. It is also possible to chirp the pulse with a wiggler taper, a feature that could be exploited for single-cycle infrared pulse production.

In conclusion, we have demonstrated the generation of a phase-stable quasi-single-cycle infrared energy modulation of an electron bunch in a wiggler. The modulation is induced by the interaction of the electrons with coherent radiation from the tail of the electron bunch. The quasi-single-cycle structure is largely due to strong diffraction along the wiggler, which lowers the field intensity experienced by the electrons far from the bunch tail. The modulation is a few MeV in amplitude and stable in phase and period at the 100 as level.

This method enables enhanced-SASE operation of LCLS for attosecond x-ray pulse production, a topic discussed elsewhere [42]. The self-modulation process also results in the generation of a gigawatt-scale CEP-stable infrared pulse that is timed to the electron bunch with subfemtosecond stability. Finally, this passive modulation method is applicable to the next generation of high-repetition rate, high average power x-ray free-electron lasers.

The authors thank C. Mayes, C. Emma, and G. Stupakov for the fruitful discussions on modeling self-modulation. This work was supported by U.S. Department of Energy (DOE) Contract No. DE-AC02-76SF00515, DOE Basic Energy Sciences Field Work Proposal No. 100317, DOE Laboratory Directed Research and Development No. DE-AC02-76SF00515, and the Robert Siemann Graduate Fellowship. The authors would like to acknowledge the OSIRIS Consortium, consisting of UCLA and IST (Lisbon, Portugal), for providing access to the OSIRIS4.0 framework. Work supported by NSF Grant No. ACI-1339893.

*jmacart@slac.stanford.edu

†marinelli@slac.stanford.edu

- [1] P. Emma, R. Akre, J. Arthur, R. Bionta, C. Bostedt, J. Bozek, A. Brachmann, P. Bucksbaum, R. Coffee, F.-J. Decker *et al.*, *Nat. Photonics* **4**, 641 (2010).
- [2] T. Ishikawa, H. Aoyagi, T. Asaka, Y. Asano, N. Azumi, T. Bizen, H. Ego, K. Fukami, T. Fukui, Y. Furukawa *et al.*, *Nat. Photonics* **6**, 540 (2012).
- [3] I. Ko, H.-S. Kang, H. Heo, C. Kim, G. Kim, C.-K. Min, H. Yang, S. Baek, H.-J. Choi, G. Mun *et al.*, *Appl. Sci.* **7**, 479 (2017).

- [4] C. Milne, T. Schietinger, M. Aiba, A. Alarcon, J. Alex, A. Anghel, V. Arsov, C. Beard, P. Beaud, S. Bettoni *et al.*, *Appl. Sci.* **7**, 720 (2017).
- [5] T. Tschentscher, C. Bressler, J. Grünert, A. Madsen, A. Mancuso, M. Meyer, A. Scherz, H. Sinn, and U. Zastra, *Appl. Sci.* **7**, 592 (2017).
- [6] C. Bostedt, S. Boutet, D. M. Fritz, Z. Huang, H. J. Lee, H. T. Lemke, A. Robert, W. F. Schlotter, J. J. Turner, and G. J. Williams, *Rev. Mod. Phys.* **88**, 015007 (2016).
- [7] A. M. Kondratenko and E. L. Saldin, *Part. Accel.* **10**, 207 (1980).
- [8] R. Bonifacio, C. Pellegrini, and L. Narducci, *Opt. Commun.* **50**, 373 (1984).
- [9] F. Krausz and M. Ivanov, *Rev. Mod. Phys.* **81**, 163 (2009).
- [10] P. H. Bucksbaum, *Science* **317**, 766 (2007).
- [11] P. Emma, K. Bane, M. Cornacchia, Z. Huang, H. Schlarb, G. Stupakov, and D. Walz, *Phys. Rev. Lett.* **92**, 074801 (2004).
- [12] S. Huang, Y. Ding, Y. Feng, E. Hemsing, Z. Huang, J. Krzywinski, A. A. Lutman, A. Marinelli, T. J. Maxwell, and D. Zhu, *Phys. Rev. Lett.* **119**, 154801 (2017).
- [13] J. Rosenzweig, D. Alesini, G. Andonian, M. Boscolo, M. Dunning, L. Faillace, M. Ferrario, A. Fukusawa, L. Giannessi, E. Hemsing *et al.*, *Nucl. Instrum. Methods Phys. Res., Sect. A* **593**, 39 (2008).
- [14] S. Reiche, P. Musumeci, C. Pellegrini, and J. Rosenzweig, *Nucl. Instrum. Methods Phys. Res., Sect. A* **593**, 45 (2008).
- [15] Y. Ding, A. Brachmann, F.-J. Decker, D. Dowell, P. Emma, J. Frisch, S. Gilevich, G. Hays, P. Hering, Z. Huang *et al.*, *Phys. Rev. Lett.* **102**, 254801 (2009).
- [16] E. Prat, F. Löhl, and S. Reiche, *Phys. Rev. ST Accel. Beams* **18**, 100701 (2015).
- [17] A. A. Lutman, T. J. Maxwell, J. P. MacArthur, M. W. Guetg, N. Berrah, R. N. Coffee, Y. Ding, Z. Huang, A. Marinelli, S. Moeller *et al.*, *Nat. Photonics* **10**, 745 (2016).
- [18] E. L. Saldin, E. A. Schneidmiller, and M. V. Yurkov, *Phys. Rev. ST Accel. Beams* **9**, 050702 (2006).
- [19] A. A. Zholents, *Phys. Rev. ST Accel. Beams* **8**, 040701 (2005).
- [20] T. Tanaka, *Phys. Rev. Lett.* **110**, 084801 (2013).
- [21] C. H. Shim, Y. W. Parc, S. Kumar, I. S. Ko, and D. E. Kim, *Sci. Rep.* **8**, 7463 (2018).
- [22] E. Hemsing, G. Stupakov, D. Xiang, and A. Zholents, *Rev. Mod. Phys.* **86**, 897 (2014).
- [23] Y. Fu, K. Midorikawa, and E. J. Takahashi, *Sci. Rep.* **8**, 7692 (2018).
- [24] E. Saldin, E. Schneidmiller, and M. Yurkov, *Nucl. Instrum. Methods Phys. Res., Sect. A* **398**, 373 (1997).
- [25] E. Saldin, E. Schneidmiller, and M. Yurkov, *Nucl. Instrum. Methods Phys. Res., Sect. A* **417**, 158 (1998).
- [26] J. Wu, T. O. Raubenheimer, and G. V. Stupakov, *Phys. Rev. ST Accel. Beams* **6**, 040701 (2003).
- [27] See Supplemental Material at <http://link.aps.org/supplemental/10.1103/PhysRevLett.123.214801> for details on the line-charge model and a complimentary paraxial model of self-modulation, which includes Refs. [28–31].
- [28] K.-J. Kim, Z. Huang, and R. Lindberg, *Synchrotron Radiation and Free-Electron Lasers: Principles of Coherent X-Ray Generation* (Cambridge University Press, Cambridge, England, 2017).
- [29] A. Hofmann, *The Physics of Synchrotron Radiation* (Cambridge University Press, Cambridge, England, 2004).
- [30] H. Wiedemann, *Particle Accelerator Physics*, 3rd ed. (Springer, Berlin, 2007).
- [31] G. Geloni, E. Saldin, E. Schneidmiller, and M. Yurkov, [arXiv:physics/0502120](https://arxiv.org/abs/physics/0502120).
- [32] R. A. Fonseca, L. O. Silva, F. S. Tsung, V. K. Decyk, W. Lu, C. Ren, W. B. Mori, S. Deng, S. Lee, T. Katsouleas *et al.*, in *Computational Science—ICCS 2002*, Vol. 2331 (Springer, Berlin, 2002), pp. 342–351.
- [33] G. Geloni, E. Saldin, E. Schneidmiller, and M. Yurkov, *Nucl. Instrum. Methods Phys. Res., Sect. A* **583**, 228 (2007).
- [34] C. Behrens, F.-J. Decker, Y. Ding, V. A. Dolgashev, J. Frisch, Z. Huang, P. Krejcik, H. Loos, A. Lutman, T. J. Maxwell *et al.*, *Nat. Commun.* **5**, 3762 (2014).
- [35] Y. Ding, K. L. F. Bane, W. Colocho, F.-J. Decker, P. Emma, J. Frisch, M. W. Guetg, Z. Huang, R. Iverson, J. Krzywinski *et al.*, *Phys. Rev. Accel. Beams* **19**, 100703 (2016).
- [36] Z. Zhang, J. Duris, J. P. MacArthur, Z. Huang, and A. Marinelli, *Phys. Rev. Accel. Beams* **22**, 050701 (2019).
- [37] J.-L. Vay, *Phys. Rev. Lett.* **98**, 130405 (2007).
- [38] J.-L. Vay, E. Cormier-Michel, W. Fawley, and C. Geddes, in *Proceedings of the 1st International Particle Accelerator Conference (IPAC 2010), Kyoto, Japan, 2010*, edited by A. Noda, Ch. Petit-Jean-Genaz, V. Schaa, T. Shirai, and A. Shirakawa (JACoW, Geneva, 2010), p. 1874.
- [39] W. Fawley and J.-L. Vay, in *Proceedings of the 32nd Free Electron Laser International Conference (FEL 2010), Malmö, Sweden, 2010*, edited by L. Liljeby (JACoW, Geneva, 2010), p. 48.
- [40] P. Emma, https://portal.slac.stanford.edu/sites/lclscore_public/LTU%20Documents/DL2-tweaker-quads.pdf.
- [41] M. P. Minitti, J. S. Robinson, R. N. Coffee, S. Edstrom, S. Gilevich, J. M. Glowina, E. Granados, P. Hering, M. C. Hoffmann, A. Miahnahri *et al.*, *J. Synchrotron Radiat.* **22**, 526 (2015).
- [42] J. Duris, S. Li, T. Driver, E. G. Champenois, J. P. MacArthur, A. A. Lutman, Z. Zhang, P. Rosenberger, J. W. Aldrich, R. Coffee *et al.*, *Nat. Photonics* **XX**, YY (2019).